How do normal faults grow?

Atle Rotevatn[a], Christopher A.-L. Jackson[b], Anette B.M. Tvedt[c], Rebecca E. Bell[b], Ingvild Blækkan[a]

[a] *Department of Earth Science, University of Bergen, PO Box 7800, 5020 Bergen, Norway*

[b] *Basins Research Group (BRG), Department of Earth Science & Engineering, Imperial College, Prince Consort Road, London, SW7 2BP, UK*

[c] *Petrolia NOCO AS, Espehaugen 32, 5258 Blomsterdalen, Norway*

**corresponding author: atle.rotevatn@uib.no (A. Rotevatn), phone: +47 48109959.*

Keywords: normal fault; fault growth; isolated fault model; coherent fault model; constant-length fault model; fault scaling

Abstract

Faults grow via a sympathetic increase in their displacement and length (isolated fault model), or by rapid length establishment and subsequent displacement accrual (constant-length fault model). To test the significance and applicability of these two models, we use time-series displacement (D) and length (L) data extracted for faults from nature and experiments. We document a range of fault behaviours, from sympathetic D-L fault growth (isolated growth) to sub-vertical D-L growth trajectories (constant-length growth). Most faults, however, are characterized by hybrid growth over two stages, dominated by (i) fault lengthening (20-30% of fault life) and (ii) displacement accrual (70-80% of fault life), respectively. Fault growth throughout the lengthening stage, during which significant displacement may also accumulate (10-60%), is achieved through rapid tip propagation, segment linkage and relay growth and breaching, best described by the isolated model. The subsequent growth stage is dominated by displacement accrual and is best described by the constant-length model. We also show that, despite being used primarily in support of the isolated fault model, global displacement-length (D-L) datasets are equally compatible with the constant-length fault model. Future research efforts should focus

on better capturing the presently poorly-documented early lengthening phase of normal fault growth.

1. Introduction

There are currently two competing models describing the growth of normal faults herein termed the 'isolated' and 'constant-length' fault models (e.g., Walsh et al., 2002; Walsh et al., 2003; Nicol et al., 2005; Jackson and Rotevatn 2013; Henstra et al., 2015; Fossen and Rotevatn 2016; Nicol et al., 2016; Tvedt et al., 2016; Childs et al., 2017; Jackson et al., 2017) (Fig. 1). The isolated model suggests fault growth occurs via a sympathetic increase in fault length and displacement (e.g., Walsh and Watterson 1988; Dawers et al., 1993; Cartwright et al., 1995; Walsh et al., 2003), whereas the constant-length model suggests faults establish their near-final lengths early in their slip history, after which they grow mainly by displacement accrual (e.g., Walsh et al. 2003; Nicol et al., 2005; Jackson and Rotevatn 2013). Being able to differentiate between the two fault growth models, and assessing their applicability, is critically important, since the way in which faults grow and interact represent a key control on (i) the development of sedimentary basins and their physiography (e.g., Gawthorpe and Leeder 2000; Jackson et al., 2017), (ii) patterns of sediment dispersal and accommodation (e.g., Ge et al., 2017; Henstra et al., 2017), and (iii) may also control the location, magnitude and recurrence interval of potentially hazardous earthquakes (Walsh et al., 2003; Nicol et al., 2005; Soliva et al., 2008; Nicol et al., 2010). Here we review, compare, and contrast these models by reappraising the wealth of data published during the past 40 years, and by describing and interpreting new data from natural and experimental fault systems. Despite typically being viewed as mutually exclusive, we here demonstrate both models accurately describe a range of fault behaviours observed in nature and experiments. We conclude that most ancient normal faults, for which appropriate kinematic constraints are available, are characterized by: (i) an initial stage of length establishment (~20-30% of the total fault lifespan), characterized by rapid tip propagation, relay formation, -breaching and segment linkage, best described by the isolated model; this stage typically also involves accumulation of c. 10-60% of the final fault displacement; (ii) a subsequent stage of displacement accrual without significant further fault lengthening, best described by the constant-length model (~70-80% of the total fault lifespan). We also show that, despite being used primarily in support of the isolated fault model, global displacement-length (D-L) datasets are equally compatible with the constant-length fault model. Major advances in our understanding of how normal faults grow may lie in us using natural examples to document the structural and kinematic characteristics of the initial stage of fault propagation and lengthening. This stage is presently insufficiently understood and poorly documented due to: (i) a lack of reliable, preserved constraints from syn-kinematic growth strata; and/or (ii) the fact that any growth strata deposited during the initial, relatively short-lived state of fault growth may simply be to thin to detect using all but the highest-resolution geophysical methods (Jackson et al., 2017).

2. The isolated fault model

The term 'isolated fault model' (Fig. 1A) was first used by Walsh et al. (2003) to describe a model by which faults grow via a sympathetic increase in their displacement and length (Fig. 1C), i.e. the view that when faults accrue displacement they also lengthen via tip propagation and linkage by relay formation and breaching (e.g., Cartwright et al., 1995; Cowie et al., 2000; Kim and Sanderson 2005; Bergen and Shaw 2010). The isolated model is supported by several studies of natural fault systems (Peacock and Sanderson 1991, 1994; Trudgill and Cartwright 1994; Wojtal 1996; Marchal et al., 1998; Morewood and Roberts 1999; Dawers and Underhill 2000; Gawthorpe and Leeder 2000; McGill et al., 2000; McLeod et al., 2000; Young et al., 2003; Soliva and Benedicto 2004; Commins et al., 2005; Hus et al., 2006; Bastesen and Rotevatn 2012), in addition to the results of numerical models (e.g. Crider and Pollard 1998; Gupta et al., 1998; Cowie et al., 2000) and analogue experiments (e.g., McClay 1990; McClay and White 1995; Ackermann et al., 2001; Clifton and Schlische 2001; Mansfield and Cartwright 2001; Acocella et al., 2005; Bellahsen and Daniel 2005).

The isolated model is largely based on the observation that, when plotted in log-log space, fault displacement and length data appear strongly positively correlated across several orders of magnitude. This empirical relationship is described as $D=cL^n$, where *D* is maximum fault displacement, *L* fault-trace length, *c* a constant, and *n* falls between 1 and 1.5 (e.g., Walsh and Watterson 1988; Cowie and Scholz 1992b; Dawers et al., 1993; Schlische et al., 1996; Schultz et al., 2008; Torabi and Berg 2011; Rotevatn and Fossen 2012). Regardless of the exact value of *n*, the empirical relationship between *D* and *L* has historically been assumed to suggest that an increase in fault displacement (*D*) is associated with a corresponding increase in fault length (*L*) (Watterson 1986; Morley et al., 1990; Peacock and Sanderson 1991; Cowie and Scholz 1992b; Cowie and Scholz 1992a; Cartwright et al., 1995; Dawers and Anders 1995; Huggins et al., 1995; Peacock and Sanderson 1996; McLeod et al., 2000; Mansfield and Cartwright 2001; Rykkelid and Fossen 2002; Kim and Sanderson 2005; Baudon and Cartwright 2008). In addition to fault displacement and length being positively correlated, support for the isolated fault model includes: (i) the occurrence of breached relays and multiple displacement minima along strike of normal faults (e.g., Gawthorpe and Leeder 2000); and (ii) theoretical fracture mechanics, which predicts that for a given rock shear strength, displacement and length must increase linearly (Cowie and Scholz 1992b). The view that faults grow through the lengthening and amalgamation of individual segments means the isolated model is also commonly referred to as 'fault growth by segment linkage', or derivations thereof (e.g., Cartwright et al., 1995; Cartwright et al., 1996; McGill et al., 2000; Jackson et al., 2002). It would be fair to say that the isolated model has dominated the structural geology and tectonics literature for decades.

Despite the fact it offers a relatively simple and thus appealing explanation of global D-L scaling relationships, there are a number of challenges to the isolated model. First, we know of no presently active or extinct (i.e. ancient) natural fault system, for which robust kinematic constraints have been presented (e.g. growth strata or geomorphic evidence documenting tip propagation and fault lengthening), that present faults that are growing or grew in accordance with the isolated fault model over geological timespans (i.e. 10^4-10^6 years; Jackson et al., 2017). Second, the isolated model does not accurately predict the (generally much lower) displacement-length ratios of individual earthquakes (e.g., Wells and Coppersmith 1994; Walsh et al., 2002; Nicol et al., 2005).

3. The constant-length fault model

The 'constant-length fault model' (Fig. 1B) was initially conceived by the Fault Analysis Group (FAG), University of Liverpool and then subsequently University College Dublin, developing in a series of papers published during the last ~15 years. At least partly motivated by the said mismatch between fault and earthquake scaling properties, Walsh et al. (2002) presented an "alternative model" for the growth of normal faults. They argued that, contrary to the isolated model, in which displacement and length increase in concert, *"(...)fault lengths are near constant from an early stage and growth is achieved mainly by increase in cumulative displacement"* (Fig. 2D). This seminal paper was quickly succeeded by a second paper (Walsh et al., 2003), which refined, expanded, and rebranded the new fault growth model, terming it the "coherent fault model" (see also Childs et al., 1995; Schöpfer et al., 2006; Schöpfer et al., 2007; Giba et al., 2012). A key concept arising from (Walsh et al., 2003) is that fault segments, which in map-view may appear isolated, may in fact, in 3D, represent components of a single, *geometrically- and kinematically-coherent* structure from their inception (see also Walsh and Watterson 1991). In 2005, Nicol et al. introduced the term 'the constant fault-length model' to explicitly capture the fact that, for much of their life, the studied faults experienced displacement accumulation rather than lengthening (Walsh et al., 2002). From here on we refer to the coherent/constant-length suite of models only as the constant-length model.

Most early work on the constant-length model was based on the analysis of growth strata preserved next to relatively large (e.g. several kilometres in length, several hundreds of metres of displacement), ancient faults imaged in 3D seismic reflection data (Meyer et al., 2002; Walsh et al., 2002). Mounting support for the constant-length fault model came from similar, seismic reflection-based studies (e.g., Giba et al., 2012; Jackson and Rotevatn 2013; Tvedt et al., 2016; Jackson et al., 2017), as well as from numerical models (e.g., Finch and Gawthorpe 2017) and analogue experiments (e.g., Schlagenhauf et al., 2008). Recent work has also used damage zone geometry, and the scaling properties of exposed, relatively small-scale (i.e. up to several metres of displacement), strike-slip faults, to provide additional support for the constant-length model (Nicol et al., 2016).

The constant-length model is attractive in that it offers a more dynamic view of D-L scaling relationships (i.e. they change over time as the fault grows; Rotevatn and Fossen 2012; Nicol et al., 2016), offering an explanation for the apparent mismatch between fault and earthquake-rupture scaling relationships (Nicol et al., 2005). However, the constant-length model initially appears at odds with the observation that relatively few ancient faults plot *below* the main trendline observed in global D-L compilations; such faults should at least theoretically occur if we assume some ancient faults became inactive early in their development, shortly after the initial phase of lengthening, or, in the case of still-active faults, they are relatively immature.

Taking the name (i.e. 'constant-length') and the key underpinning concept (i.e. displacement accrual without significant further lengthening) at face value, it seems obvious the constant-length model would preclude significant tip propagation for the majority of a fault's lifespan. In a recent paper, however, Childs et al. (2017) recognise two sub-sets of this basic model; the 'constant-length coherent model' and a 'propagating coherent growth model'. Although Childs et al. (2017) attempt to clarify the terminology related to the key fault growth models, we propose the redefinition of the underpinning key concepts rather confuses matters. For example, tip propagation is widely considered a key diagnostic of the isolated fault model (e.g., Jackson et al., 2017); the introduction of tip propagation in the 'propagating coherent growth model' (Childs et al., 2017) therefore effectively makes it harder to test whether a fault grew according to the isolated or the constant-length model. As such, we argue that, by identifying two sub-sets, Childs et al. (2017) leave the constant-length model without a set of clear, testable criteria.

Motivated by the above review, and the fact the two models have co-existed for ~15 years, we find it timely to critically assess their relative importance for describing the growth of normal faults. To do this we study seismically imaged natural normal faults, in addition to faults generated in analogue models, to extract D-L data through time. D-L data for individual faults *through time* is key to understanding fault growth, since the global D-L database really only shows a static view, where each datapoint represents the final step of what is essentially a fault's unknown journey through D-L space (Nicol et al., 2010; Rotevatn and Fossen 2012; Nicol et al., 2016). With these data we specifically aim to: (i) elucidate the poorly-documented lengthening phase of faults exhibiting an overall constant-length behaviour; (ii) reassess the isolated and constant-length models in an attempt to present a unified model for normal fault growth; and (iii) to suggest some key questions to be addressed in future research.

4. Fault behaviour in D-L space through time

To reveal how faults grow in space and time, we present D-L data extracted at several points in the growth history of natural and experimentally reproduced faults (Fig. 2). Data from natural faults are derived from throw backstripping of, and analysis of growth strata from, syn-sedimentary growth faults from the Egersund Basin, offshore Norway (Tvedt et al., 2013; Tvedt et al., 2016) and the Santos Basin, offshore Brazil (Tvedt 2016) (see cited papers and Jackson et al. 2017 for backstripping method used and justification). Additional D-L data from natural faults were extracted from Meyer et al. (2002), and data from physical experiments from sandbox (Schlagenhauf et al., 2008) and new plaster models (Blækkan 2016).

The plots of D-L evolution through time (Fig. 2) clearly show that only few natural and experimental faults behave according to the predictions of the isolated model, i.e. they display a sympathetic increase in length as displacement is accrued (see inset *i* in Fig. 2A). This observation, in concert with those from previous studies (e.g., Cartwright et al., 1996; McLeod et al., 2000; Commins et al., 2005), suggests that fault growth according to the isolated fault model does occur, but is an end-member behaviour rather than the norm.

Much more commonly, faults exhibit a growth path that can be split into an early, relatively low-gradient segment, and a subsequent, relatively high-gradient segment, separated by a relatively well-defined, relatively abrupt inflection point (see inset *ii* in Fig. 2A). The high-gradient segment is typical of fault behaviour according to the constant-length fault model, whereby near-vertical growth trends in D-L space represent displacement accrual without significant fault lengthening (Meyer et al., 2002; Walsh et al., 2002). However, the preceding and relatively lower-gradient segments of the D-L graphs (Fig. 2A) exhibit great spread. For example, the D-L plots in Figure 2 show that the initial lengthening stage often involves not only lengthening, but may also involve (periods of) significant displacement accrual (up to 40-60% of the total displacement). The amount of displacement accrual varies, and the gradients in D-L space during this early stage of growth therefore vary greatly, from relatively gentle, constant-length-like gradients to steeper, isolated-like gradients (Fig. 2). These data thus suggest that the initial lengthening stage is more complex than suggested by the constant-length model (e.g., Walsh et al., 2002) and leads to the question "what style of growth (i.e. instantaneous length establishment vs. lengthening by tip propagation and linkage) characterizes the relatively low-gradient phase seen in the D-L paths, and is the 'lengthening' stage adequately captured and understood in the present models for normal fault growth?".

As discussed by Childs et al. (2017) and Jackson et al., (2017), seismic reflection-based investigations of faults may show that faults establish their lengths within the first resolvable time increment but that, because this increment may be longer than the lengthening stage, the latter goes undetected. To investigate the lengthening stage further we therefore return to physical analogue experiments, in which this early stage of fault growth may be closely monitored and captured. In the following we discuss a plaster experiment (Figs. 3 and 4) of Blækkan (2016), first showing images of the experiment at relatively long (5-second) time-steps (Fig. 3), before showing the early stages of the experiment at much shorter (0.5-second) time-steps (Fig. 4). We do this to mimic having different temporal resolutions of data (i.e. low-resolution data at 5 sec time-steps vs. high-resolution data at 0.5 sec time-steps) to show how this impacts our understanding of fault growth. For information about the experimental setup, see Blækkan (2016).

Consider Figure 3, where we show map-view image showing the evolution of a large (relative to the scale of the experiment) normal fault (F1) at 5 second intervals (timesteps T1-T4). Even after first timestep (T2), F1 has grown across the width of the model. The faults tips are pinned laterally at the experiment boundary, thus emulating natural reasons for lateral fault tip pinning, such as pinchout of mobile substrates and/or interaction with other faults. Further timesteps (T3 and T4) are characterised by displacement accrual, accompanied by rotation and breaching of relay zones. Based on viewing the experiment at a relatively low temporal resolution (i.e. 5 sec timesteps), which we compare to the limitations of the lowest resolvable time increment from growth strata when analysing fault growth in the subsurface using reflection seismic and well data, F1 thus appears to grow in accordance with the constant-length model.

By making the observational increments shorter (i.e. 0.5 secs) we can now investigate the geometric and kinematic characteristics of the lengthening phase between timesteps T1 and T2 (i.e. T1a-d; Fig. 4). A fault segment (termed main segment S1; Fig. 4), which nucleates or at least breaches the surface in the western part of the model during T1a, propagates eastward and lengthens during T1b and T1c. Fault lengthening during this stage is largely achieved by the nucleation, propagation, and linkage of new, smaller segments ahead of the propagating eastern tip of S1. In time step T1c, a second segment (termed main segment S2; Fig. 4) nucleates in the eastern part of the model, clearly separate form the main S1 structure in the west. From time step T1c to T1d, both tips of S2 propagate. Eastward propagation of S2 is arrested at the model boundary; the western tip approaches the oncoming and now-rapidly east-propagating tip of S1. At T1d, S1 and S2 remain unlinked, but are underlapping and *approaching* one another (*sensu* Peacock et al., 2017). The final 0.5 second-long timestep between T1d and T2 sees amalgamation of smaller S2 segments, which are soft-linked during T1d, but hard-linked by T2. By T2, S1 and S2 have overlapped and soft-linked, bounding a relay zone that is eventually breached by T3.

The style of fault growth documented in time steps T1a through T1d above (Fig. 4) is similar to that observed in natural fault systems (e.g., Jackson et al., 2002; Gawthorpe et al., 2003; Young et al., 2003), and is consistent with the predictions of the isolated model (e.g., Peacock and Sanderson 1991; Cartwright et al., 1995; Walsh et al., 2003). Fault segments nucleate, propagate, and link to establish the full length of the fault, and it seems clear that, despite the fact we only have a top-surface view, upon nucleation of S2, S1 and S2 are sufficiently far apart that they appear not to form part of a single, geometrically and kinematically coherent structure from their inception (see Walsh et al., 2003).

The example above also highlights that for a given fault, D-L ratios may change abruptly as the fault lengthens by linkage of precursor segments. For example, consider timestep T2 (Fig. 3), where F1 is characterised by a D-L ratio of c. 1:35. However, also consider timestep T1d (Fig. 4), where the D-L ratios of precursor proto-F1 segments are clearly higher (~1:10), as maximum displacement at this stage is divided by the (much shorter) lengths of those segment. As such, D-L ratios should be treated with care since they depend on the length-scale considered (individual segment length immediately before, vs. full fault length immediately after, amalgamation and full length establishment of a fault), and the fact this ratio is dynamic, changing with time as faults grow (Rotevatn and Fossen 2012; Nicol et al., 2016).

Finally, we return to the D-L plots discussed initially in this section and shown in Figure 2. The complex D-L paths observed in the lengthening stage may seem very different to the well-known, sub-vertical D-L growth trends from Meyer et al. (2002), which were used by Walsh et al. (2002) in support of the constant-length model. However, the extracted D-L paths from Meyer et al. (2002) show that, although sub-vertical growth trends are seen in the right part of the curves (Fig. 2D), there is an unresolved precursor stage that involves (i) not only lengthening, but a variable amount of displacement accrual (10-60% of total displacement; Fig. 2D) and (ii) lower-gradient but variable trajectories through D-L space (Fig. 2D). This important point may have been gone unnoticed previously, since the D-L data from Walsh et al. (2002) and Meyer et al. (2002) were presented only in log-log space. Plotting such data in log-log space is inherently problematic, as it may unintentionally mask variability and statistical spread. Interestingly, although the D-L paths presented in this study vary greatly, most of the D-L paths shown in Figure 5 fall within the cloud of the global D-L dataset when plotted in log-log space. This highlights the danger of plotting data on logarithmic scales, and demonstrates how radically different D-L behaviours of faults may effectively 'hide' in log-log space. It also demonstrates that the often-cited D-L correlation, when plotted on log-log scales, is largely unusable as an argument in favour of any exclusive view on how normal faults grow.

5. Conclusions and future research challenges

Using D-L data from a range of natural and experimental faults, we have demonstrated that the isolated and constant-length fault models both describe fault behaviours in nature, and as such are not mutually exclusive. The critical point is that they both appear to describe behaviours at specific points in the evolution of a fault; i.e. the isolated model, defined by tip propagation and segment linkage, characterises the initial part of the fault lifespan when its growth is dominated by lengthening, whereas the constant-length model characterises the latter part of the faults evolution, when growth is dominated by displacement accrual.

We thus conclude that normal faults are generally characterized by a hybrid growth behaviour (Fig. 6), whereby a rapid stage of fault propagation, linkage, and lengthening (Stage 1; lengthening stage) is followed by a stage of constant-length displacement accrual (Stage 2; displacement accrual stage). The first stage is best described by the isolated fault model, in that it involves tip propagation, segment linkage, and overall fault lengthening. Importantly, the lengthening stage may also involve displacement accrual, and the gradient of the growth path during this stage may range from sub-vertical ('constant-length'-type gradient; trajectory 'a' in Fig. 6) to sub-horizontal ('isolated'-type gradient; trajectory 'e' in Fig. 6). The second stage is characterized by displacement accrual and limited fault lengthening. The D-L trajectory during this growth stage is typically sub-vertical. Hybrid-type fault behaviours such as demonstrated herein, whereby isolated and constant-length fault growth characterize successive phases of fault evolution, finds some support in previous studies (Jackson and Rotevatn 2013; Horne 2016; Finch and Gawthorpe 2017) but remains to be more widely corroborated from natural examples. The duration of each stage in the model presented above remains uncertain. Normal faults analysed by Walsh et al. (2002) and Jackson et al. (2017) established their near-final lengths within 20-33% of their slip history; similarly, the majority of experimental faults in Schlagenhauf et al. (2008) grew to near-final lengths within c. 30% of their model durations. We therefore tentatively conclude that, irrespective of their final size, faults typically spend 20-30% of their lifespan in the lengthening phase (Stage 1), before accruing displacement for the remainder of their slip histories (Stage 2).

A critical research task to deepen the understanding of normal fault growth lies in undertaking more displacement backstripping studies of seismically imaged growth faults in order to investigate faults' D-L trajectories through time. Furthermore, new insight may be gained from reassessing the global D-L dataset to sort, examine and analyse the data based on variables such as tectonic setting, strain rate and host lithology in order to elucidate any controls on fault behaviour.

A key future research challenge related to the growth of normal faults is to better document the initial lengthening phase described above. Insights may be gained by integrating geophysical imaging techniques (e.g. reflection, sparker, pinger, boomer, and chirp profiling), which allow mapping of fault structure and associated growth strata, and borehole data, which constrain the age of the growth strata and thus the timescale of fault development (e.g., Taylor et al., 2004; Nicol et al., 2005). Note that, in some active rifts, such as the Gulf of Corinth, Greece (e.g., Nixon et al., 2016; Bell et al., 2017; Gawthorpe et al., 2017), basin underfilling represents a drawback to the investigation of normal fault growth based on the analysis of growth strata (see discussion by Jackson et al. 2017).

Despite our tentative conclusion that the lengthening stage typically endures for 20-30% of fault lifespan, the duration of each stage of the above mentioned hybrid fault model remains uncertain, and more research is needed to fully understand what the notion of 'rapid' lengthening (e.g., Walsh et al., 2002) really entails. We speculate that the significant variability of D-L trajectories demonstrated for the lengthening stage (Stage 1) may translate to a similar variability in its duration. We further suggest that investigations into the duration of the lengthening stage should encompass the full spectrum of fault sizes in nature and experiments, to rigorously test whether duration is linked to fault size, despite the fact that we herein have tentatively concluded that it is not.

Acknowledgements

The geology department at the University of Otago, New Zealand, is thanked for hosting the first author for a research sabbatical, during which time this paper was written.

FIGURE TEXT CAPTIONS:

Figure 1. Conceptual models for the development of blind normal fault systems: (a) the isolated fault model (Walsh and Watterson 1988; Cartwright et al., 1995; Dawers and Anders 1995; Huggins et al., 1995); and (b) the constant-length fault model (Childs et al., 1995; Walsh et al., 2002; Walsh et al., 2003; Giba et al., 2012). The (i) plan-view, (ii) strike-projection and (iii) displacement–length (D–L) plots are shown to illustrate the key geometrical and evolutionary aspects of each model. The black arrows in (ii) show the fault level of the map shown in (i). F1-3, faults 1–3; T1-3, time-steps 1–3. Note that, based on the final fault length (i.e. T3 in i), shape (i.e. T3 in ii) and throw distribution (i.e. T3 in iii), it is difficult to determine which growth model best describes its evolution. (c) Schematic D-L plots through fault life according to the isolated fault model; time steps correspond to those shown in (a). (c) Schematic D-L plots through fault life according to the constant-length fault model; time steps correspond to those shown in (b). (a) and (b) are from Jackson et al. (2017); (c) and (d) are modified from Nicol et al. (2016).

Figure 2. Normalized maximum displacement (D) versus normalized fault length (L) plots though fault life for a series of faults. (A) shows data from all faults studied herein, whereas (B), (C), and (D) show selections of the data. The data includes natural faults from Tvedt et al. (2013, 2016), Tvedt (2016), Meyer et al. (2002), faults from plaster experiments by Blækkan (2016) and faults from sandbox experiments by Schlagenhauf et al. (2008). Note that the data from Meyer et al. (2002) carries some uncertainty as the data were manually extracted from the log-log D-L plots in that paper. Inset (i) shows D-L graphs for select faults that exhibit sympathetic D-L growth, i.e. isolated fault growth. Inset (ii) shows D-L graphs from select faults that show clearly separate low-gradient and high-gradient segments, separated by clear inflection points. (B) shows data from natural faults extracted from Tvedt (2016) and Tvedt et al. (2013, 2016). (C) shows data from faults produced in physical analogue

experiments from Schlagenhauf et al. (2008) and Blækkan (2016). (D) shows the data extracted from Meyer et al. (2002); note however that we have added (x, y) = (0, 0) to all the D-L curves, in order to illustrate that each of the vertical D-L graphs in Meyer et al. (2002) have an additional unrecorded and unknown growth phase that is illustrated by dashed lines. See text for full discussion.

Figure 3. Plaster experiment of normal fault evolution. Four timesteps, T1 through T4 at 5 second intervals, are shown. Timestep T1 is the experiment at the onset of extension. To the right, displacement-length plots for the fault evolving in the experiment are shown for timesteps T2 (green), T3 (blue) and T4 (red). Note that the fault seen in T2 already at that stage has established itself across the extent of the model. See Figure 4 for four additional, shorter, 0.5-second timesteps immediately prior to timestep T2, which show the lengthening phase of the fault.

Figure 4. Plaster experiment of normal fault evolution; 4 timesteps are shown at 0.5 second intervals; T1a through T1d. These timesteps cover the 2 seconds leading up to timestep T2 in Figure 3; see Figure 3 caption for further explanation.

Figure 5. Global D-L dataset (grey data points) for faults plotted in log-log space (D-L data extracted from Krantz 1988; Gudmundsson and Bäckström 1991; Cowie and Scholz 1992a, and references therein; Dawers et al., 1993; Cartwright et al., 1995; Schlische et al., 1996; Schultz and Fossen 2002). The D-L paths shown in Figure 2 of this study are also shown. Note most of the different D-L paths from this study plot within the global dataset, despite that these growth paths show a wide range of behaviours (see text for full discussion). This demonstrates that the global correlation of D and L cannot be invoked to support 'isolated' fault growth, since 'constant-length' and hybrid growth patterns are all fully consistent with, and may hide within, the global D-L database as shown here.

Figure 6. Schematic illustration showing idealized D-L growth trajectories of the end member 'isolated' (green) and 'constant-length' (blue) fault models, as well as a series of hybrid-type fault growth trajectories (black). As shown in this paper, few faults follow the isolated or constant-length trajectories; most faults follow D-L growth paths that are characteristic of a hybrid growth mode characterized by two stages. The

first stage is characterized by rapid fault lengthening and a variable amount of displacement accrual, and is best described by the isolated model since it is associated with lengthening achieved by tip propagation, relay formation and breakdown, segment linkage and amalgamation to ultimately establish near-full fault lengths at the end of Stage 1. The second stage (Stage 2), is best described as 'constant-length' fault behaviour, i.e. displacement accrual without significant tip propagation or further fault lengthening. The fault growth trajectory in D-L space during Stage 1 of the hybrid growth model varies significantly, from sub-horizontal coherent-like trajectories with limited displacement accrual (graph a), to steep and isolated-like trajectories with significant displacement accrual during Stage 1 (graph e). See text for full discussion.

REFERENCES

Ackermann, R. V., Schlische, R. W. & Withjack, M. O. 2001. The geometric and statistical evolution of normal fault systems: an experimental study of the effects of mechanical layer thickness on scaling laws. *Journal of Structural Geology* **23**(11), 1803-1819.

Acocella, V., Morvillo, P. & Funiciello, R. 2005. What controls relay ramps and transfer faults within rift zones? Insights from analogue models. *Journal of Structural Geology* **27**(3), 397-408.

Bastesen, E. & Rotevatn, A. 2012. Evolution and structural style of relay zones in layered limestone–shale sequences: insights from the Hammam Faraun Fault Block, Suez rift, Egypt. *Journal of the Geological Society* **169**(4), 477-488.

Baudon, C. & Cartwright, J. A. 2008. 3D seismic characterisation of an array of blind normal faults in the Levant Basin, Eastern Mediterranean. *Journal of Structural Geology* **30**(6), 746-760.

Bell, R. E., Duclaux, G., Nixon, C. W., Gawthorpe, R. L. & McNeill, L. C. 2017. High-angle, not low-angle, normal faults dominate early rift extension in the Corinth Rift, central Greece. *Geology*.

Bellahsen, N. & Daniel, J. M. 2005. Fault reactivation control on normal fault growth: an experimental study. *Journal of Structural Geology* **27**(4), 769-780.

Bergen, K. J. & Shaw, J. H. 2010. Displacement profiles and displacement-length scaling relationships of thrust faults constrained by seismic-reflection data. *Geological Society of America Bulletin* **122**(7-8), 1209-1219.

Blækkan, I. 2016. Evolution of normal faults and fault-related damage: insights from physical experiments. Unpublished MSc thesis thesis, University of Bergen, Norway.

Cartwright, J. A., Mansfield, C. S. & Trudgill, B. D. 1996. Fault growth by segment linkage. In: *Modern developments in structural interpretations* (edited by Buchanan, P. C. & Nieuwland, D. A.). *Geological Society, London, Special Publications* **99**, 163-177.

Cartwright, J. A., Trudgill, B. D. & Mansfield, C. S. 1995. Fault growth by segment linkage: an explanation for scatter in maximum displacement and trace length data from the Canyonlands Grabens of SE Utah. *Journal of Structural Geology* **17**, 1319-1326.

Childs, C., Holdsworth, R. E., Jackson, C. A. L., Manzocchi, T., Walsh, J. J. & Yielding, G. 2017. Introduction to the geometry and growth of normal faults. *Geological Society, London, Special Publications*, SP439.23.

Childs, C., Watterson, J. & Walsh, J. J. 1995. Fault overlap zones within developing normal fault systems. *Journal of the Geological Society, London* **152**, 535-549.

Clifton, A. E. & Schlische, R. W. 2001. Nucleation, growth, and linkage of faults in oblique rift zones: Results from experimental clay models and implications for maximum fault size. *Geology* **29**(5), 455-458.

Commins, D., Gupta, S. & Cartwright, J. 2005. Deformed streams reveal growth and linkage of a normal fault array in the Canyonlands graben, Utah. *Geology* **33**(8), 645-648.

Cowie, P. A., Gupta, S. & Dawers, N. H. 2000. Implications of fault array evolution for synrift depocentre development: insights from a numerical fault growth model. *Basin Research* **12**(3-4), 241-261.

Cowie, P. A. & Scholz, C. H. 1992a. Displacement-length scaling relationship for faults: data synthesis and discussion. *Journal of Structural Geology* **14**(10), 1149-1156.

Cowie, P. A. & Scholz, C. H. 1992b. Physical explanation for the displacement-length relationship of faults, using a post-yield fracture mechanics model. *Journal of Structural Geology* **14**, 1133-1148.

Crider, J. G. & Pollard, D. D. 1998. Fault linkage: Three-dimensional mechanical interaction between echelon normal faults. *J. Geophys. Res.* **103**(B10), 24373-24391.

Dawers, N. H. & Anders, M. H. 1995. Displacement-length scaling and fault linkage. *Journal of Structural Geology* **17**(5), 607-614.

Dawers, N. H., Anders, M. H. & Scholz, C. H. 1993. Growth of normal faults: Displacement-length scaling. *Geology* **21**(12), 1107-1110.

Dawers, N. H. & Underhill, J. R. 2000. The role of fault interaction and linkage in controlling synrift stratigraphic sequences: late Jurassic, Statfjord East Area, northern North Sea. *AAPG Bulletin* **84**, 45-64.

Finch, E. & Gawthorpe, R. 2017. Growth and interaction of normal faults and fault network evolution in rifts: insights from three-dimensional discrete element modelling. *Geological Society, London, Special Publications* **439**(1), 219-248.

Fossen, H. & Rotevatn, A. 2016. Fault linkage and relay structures in extensional settings—A review. *Earth-Science Reviews* **154**, 14-28.

Gawthorpe, R., Leeder, M., Kranis, H., Skourtsos, E., Andrews, J., Henstra, G., Mack, G., Muravchik, M., Turner, J. & Stamatakis, M. 2017. Tectono-sedimentary evolution of the Plio-Pleistocene Corinth rift, Greece. *Basin Research*.

Gawthorpe, R. L., Jackson, C. A. L., Young, M. J., Sharp, I. R., Moustafa, A. R. & Leppard, C. W. 2003. Normal fault growth, displacement localisation and the evolution of normal fault populations: the Hammam Faraun fault block, Suez rift, Egypt. *Journal of Structural Geology* **25**(6), 883-895.

Gawthorpe, R. L. & Leeder, M. R. 2000. Tectono-sedimentary evolution of active extensional basins. *Basin Research* **12**, 195-218.

Ge, Z., Nemec, W., Gawthorpe, R. L., Rotevatn, A. & Hansen, E. W. M. 2017. Response of unconfined turbidity current to relay-ramp topography: insights from process-based numerical modelling. *Basin Research*, n/a-n/a.

Giba, M., Walsh, J. & Nicol, A. 2012. Segmentation and growth of an obliquely reactivated normal fault. *Journal of Structural Geology* **39**, 253-267.

Gudmundsson, A. & Bäckström, K. 1991. Structure and development of the Sveinagja graben, northeast Iceland. *Tectonophysics* **200**(1-3), 111-125.

Gupta, S., Cowie, P. A., Dawers, N. H. & Underhill, J. R. 1998. A mechanism to explain rift-basin subsidence and stratigraphic patterns through fault-array evolution. *Geology* **26**(7), 595-598.

Henstra, G. A., Gawthorpe, R. L., Helland-Hansen, W., Ravnås, R. & Rotevatn, A. 2017. Depositional systems in multiphase rifts: seismic case study from the Lofoten margin, Norway. *Basin Research* **29**(4), 447-469.

Henstra, G. A., Rotevatn, A., Gawthorpe, R. L. & Ravnås, R. 2015. Evolution of a major segmented normal fault during multiphase rifting: The origin of plan-view zigzag geometry. *Journal of Structural Geology* **74**, 45-63.

Horne, E. 2016. Kinematics and growth of supra-salt fault systems: A field and subsurface analysis, Salt Valley Salt Wall, Paradox Basin, Utah. Unpublished MSc thesis, Colorado School of Mines.

Huggins, P., Watterson, J., Walsh, J. & Childs, C. 1995. Relay zone geometry and displacement transfer between normal faults recorded in coal-mine plans. *Journal of Structural Geology* **17**(12), 1741-1755.

Hus, R., De Batist, M., Klerkx, J. & Matton, C. 2006. Fault linkage in continental rifts: structure and evolution of a large relay ramp in Zavarotny; Lake Baikal (Russia). *Journal of Structural Geology* **28**, 1338-1351.

Jackson, C. A.-L., Bell, R. E., Rotevatn, A. & Tvedt, A. B. M. 2017. Techniques to determine the kinematics of synsedimentary normal faults and implications for fault growth models. *Geological Society, London, Special Publications* **439**.

Jackson, C. A.-L., Gawthorpe, R. L. & Sharp, I. R. 2002. Growth and linkage of the East Tanka fault zone, Suez rift: structural style and syn-rift stratigraphic response. *Journal of the Geological Society* **159**(2), 175-187.

Jackson, C. A. L. & Rotevatn, A. 2013. 3D seismic analysis of the structure and evolution of a salt-influenced normal fault zone: A test of competing fault growth models. *Journal of Structural Geology* **54**, 215-234.

Kim, Y.-S. & Sanderson, D. J. 2005. The relationship between displacement and length of faults: a review. *Earth-Science Reviews* **68**(3-4), 317-334.

Krantz, R. W. 1988. The odd-axis model: orthorombic fault patterns and three-dimensional strain fields. Unpublished PhD thesis, University of Arizona.

Mansfield, C. S. & Cartwright, J. A. 2001. Fault growth by linkage: observations and implications from analogue models. *Journal of Structural Geology* **23**, 745-763.

Marchal, D., Guiraud, M., Rives, T. & van den Driessche, J. 1998. Space and time propagation processes of normal faults. *Geological Society, London, Special Publications* **147**(1), 51-70.

McClay, K. & White, M. 1995. Analogue modelling of orthogonal and oblique rifting. *Marine and Petroleum Geology* **12**(2), 137-151.

McClay, K. R. 1990. Extensional fault systems in sedimentary basins: a review of analogue model studies. *Marine and Petroleum Geology* **7**(3), 206-233.

McGill, G. E., Schultz, R. A. & Moore, J. M. 2000. Fault growth by segment linkage: an explanation for scatter in maximum displacement and trace length data from the Canyonlands grabens of SE Utah: Discussion. *Journal of Structural Geology* **22**, 135-140.

McLeod, A. E., Dawers, N. H. & Underhill, J. R. 2000. The propagation and linkage of normal faults: insights from the Strathspey-Brent-Statfjord fault array, northern North Sea. *Basin Research* **12**, 263-284.

Meyer, V., Nicol, A., Childs, C., Walsh, J. & Watterson, J. 2002. Progressive localisation of strain during the evolution of a normal fault population. *Journal of Structural Geology* **24**(8), 1215-1231.

Morewood, N. C. & Roberts, G. P. 1999. Lateral propagation of the surface trace of the South Alkyonides normal fault segment, central Greece: its impact on models of fault growth and displacement–length relationships. *Journal of Structural Geology* **21**(6), 635-652.

Morley, C., Nelson, R., Patton, T. & Munn, S. 1990. Transfer zones in the East African rift system and their relevance to hydrocarbon exploration in rifts (1). *AAPG Bulletin* **74**(8), 1234-1253.

Nicol, A., Childs, C., Walsh, J. J., Manzocchi, T. & Schöpfer, M. P. J. 2016. Interactions and growth of faults in an outcrop-scale system. *Geological Society, London, Special Publications* **439**.

Nicol, A., Walsh, J., Berryman, K. & Nodder, S. 2005. Growth of a normal fault by the accumulation of slip over millions of years. *Journal of Structural Geology* **27**(2), 327-342.

Nicol, A., Walsh, J. J., Villamor, P., Seebeck, H. & Berryman, K. R. 2010. Normal fault interactions, paleoearthquakes and growth in an active rift. *Journal of Structural Geology* **32**(8), 1101-1113.

Nixon, C. W., McNeill, L. C., Bull, J. M., Bell, R. E., Gawthorpe, R. L., Henstock, T. J., Christodoulou, D., Ford, M., Taylor, B. & Sakellariou, D. 2016. Rapid spatiotemporal variations in rift structure during development of the Corinth Rift, central Greece. *Tectonics* **35**(5), 1225-1248.

Peacock, D., Nixon, C., Rotevatn, A., Sanderson, D. & Zuluaga, L. 2017. Interacting faults. *Journal of Structural Geology* **97**, 1-22.

Peacock, D. & Sanderson, D. 1996. Effects of propagation rate on displacement variations along faults. *Journal of Structural Geology* **18**(2-3), 311-320.

Peacock, D. C. P. & Sanderson, D. J. 1991. Displacements, segment linkage and relay ramps in normal fault zones. *Journal of Structural Geology* **13**, 721-733.

Peacock, D. C. P. & Sanderson, D. J. 1994. Geometry and development of relay ramps in normal fault systems. *AAPG Bulletin* **78**, 147-165.

Rotevatn, A. & Fossen, H. 2012. Soft faults with hard tips: magnitude-order displacement gradient variations controlled by strain softening versus hardening; implications for fault scaling. *Journal of the Geological Society* **169**(2), 123-126.

Rykkelid, E. & Fossen, H. 2002. Layer rotation around vertical fault overlap zones: observations from seismic data, field examples and physical experiment. *Marine and Petroleum Geology* **19**, 181-192.

Schlagenhauf, A., Manighetti, I., Malavieille, J. & Dominguez, S. 2008. Incremental growth of normal faults: Insights from a laser-equipped analog experiment. *Earth and Planetary Science Letters* **273**(3), 299-311.

Schlische, R. W., Young, S. S., Ackermann, R. V. & Gupta, A. 1996. Geometry and scaling relations of a population of very small rift-related normal faults. *Geology* **24**(8), 683-686.

Schöpfer, M. P., Childs, C., Walsh, J. J., Manzocchi, T. & Koyi, H. A. 2007. Geometrical analysis of the refraction and segmentation of normal faults in periodically layered sequences. *Journal of Structural Geology* **29**(2), 318-335.

Schöpfer, M. P. J., Childs, C. & Walsh, J. J. 2006. Localisation of normal faults in multilayer sequences. *Journal of Structural Geology* **28**(5), 816-833.

Schultz, R. A. & Fossen, H. 2002. Displacement-length scaling in three dimensions: the importance of aspect ratio and application to deformation bands. *Journal of Structural Geology* **24**, 1389-1411.

Schultz, R. A., Soliva, R., Fossen, H., Okubo, C. H. & Reeves, D. M. 2008. Dependence of displacement-length scaling relations for fractures and deformation bands on the volumetric changes across them. *Journal of Structural Geology* **30**(11), 1405-1411.

Soliva, R. & Benedicto, A. 2004. A linkage criterion for segmented normal faults. *Journal of Structural Geology* **26**(12), 2251-2267.

Soliva, R., Benedicto, A., Schultz, R. A., Maerten, L. & Micarelli, L. 2008. Displacement and interaction of normal fault segments branched at depth: Implications for fault growth and potential earthquake rupture size. *Journal of Structural Geology* **30**(10), 1288-1299.

Taylor, S. K., Bull, J. M., Lamarche, G. & Barnes, P. M. 2004. Normal fault growth and linkage in the Whakatane Graben, New Zealand, during the last 1.3 Myr. *Journal of Geophysical Research: Solid Earth* **109**(B2).

Torabi, A. & Berg, S. S. 2011. Scaling of fault attributes: A review. *Marine and Petroleum Geology* **28**(8), 1444-1460.

Trudgill, B. D. & Cartwright, J. A. 1994. Relay ramp forms and normal fault linkages, Canyonlands National Park, Utah. *GSA Bulletin* **106**, 1143-1157.

Tvedt, A. B. M. 2016. The geometry and evolution of supra-salt normal fault arrays. Unpublished PhD thesis thesis, University of Bergen, Norway.

Tvedt, A. B. M., Rotevatn, A. & Jackson, C. A. L. 2016. Supra-salt normal fault growth during the rise and fall of a diapir: Perspectives from 3D seismic reflection data, Norwegian North Sea. *Journal of Structural Geology* **91**, 1-26.

Tvedt, A. B. M., Rotevatn, A., Jackson, C. A. L., Fossen, H. & Gawthorpe, R. L. 2013. Growth of normal faults in multilayer sequences: A 3D seismic case study from the Egersund Basin, Norwegian North Sea. *Journal of Structural Geology* **55**, 1-20.

Walsh, J. J., Bailey, W. R., Childs, C., Nicol, A. & Bonson, C. G. 2003. Formation of segmented normal faults: a 3-D perspective. *Journal of Structural Geology* **25**(8), 1251-1262.

Walsh, J. J., Nicol, A. & Childs, C. 2002. An alternative model for the growth of faults. *Journal of Structural Geology* **24**(11), 1669-1675.

Walsh, J. J. & Watterson, J. 1988. Analysis of the relationship between displacements and dimensions of faults. *Journal of Structural Geology* **10**(3), 239-247.

Walsh, J. J. & Watterson, J. 1991. Geometric and kinematic coherence and scale effects in normal fault systems. *Geological Society, London, Special Publications* **56**(1), 193-203.

Watterson, J. 1986. Fault dimensions, displacements and growth. *Pure and Applied Geophysics* **124**(1-2), 365-373.

Wells, D. L. & Coppersmith, K. J. 1994. New empirical relationships among magnitude, rupture length, rupture width, rupture area, and surface displacement. *Bulletin of the seismological Society of America* **84**(4), 974-1002.

Wojtal, S. F. 1996. Changes in fault displacement populations correlated to linkage between faults. *Journal of Structural Geology* **18**(2-3), 265-279.

Young, M. J., Gawthorpe, R. L. & Sharp, I. R. 2003. Normal fault growth and early syn-rift sedimentology and sequence stratigraphy: Thal Fault, Suez Rift, Egypt. *Basin Research* **15**(4), 479-502.

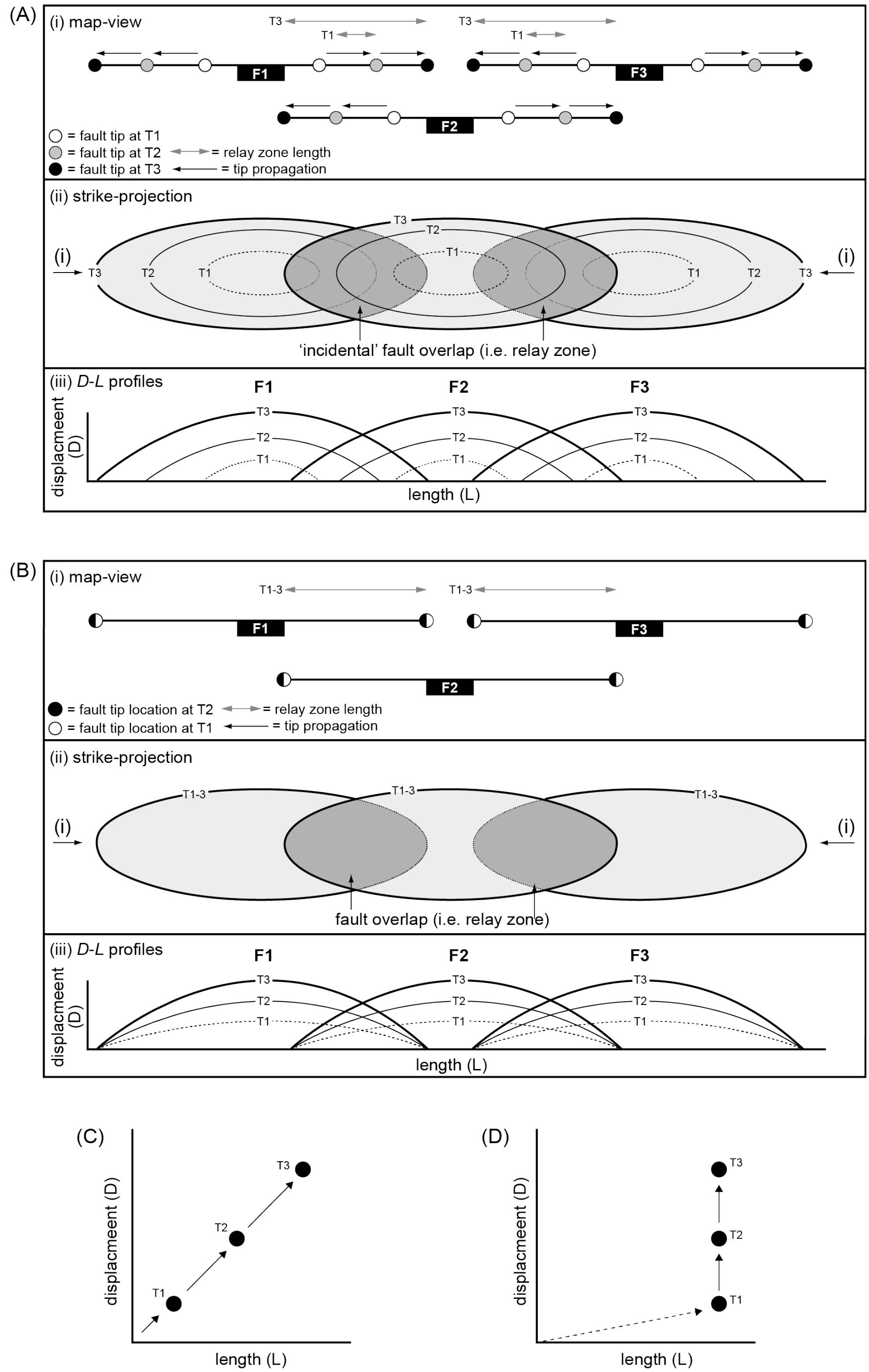

Figure 1. Conceptual models for the development of blind normal fault systems: (a) the isolated fault model (Walsh & Watterson 1988; Dawers & Anders 1995; Huggins et al. 1995; Cartwright et al. 1995); and (b) the constant-length fault model (cf. Childs et al. 1995; Walsh et al. 2002, 2003; Giba et al. 2012; see also Baudon & Cartwright 2008; Jackson & Rotevatn 2013; Nicol et al. 2016). The (i) plan-view, (ii) strike-projection and (iii) displacement–length (D–L) plots are shown to illustrate the key geometrical and evolutionary aspects of each model. The black arrows in (ii) show the fault level of the map shown in (i). F1-3, faults 1–3; T1-3, time-steps 1–3. Note that, based on the final fault length (i.e. T3 in i), shape (i.e. T3 in ii) and throw distribution (i.e. T3 in iii), it is difficult to determine which growth model best describes its evolution. (c) Schematic D-L plots through fault life according to the isolated fault model; time steps correspond to those shown in (a). (c) Schematic D-L plots through fault life according to the constant-length fault model; time steps correspond to those shown in (b). (a) and (b) are from Jackson et al. (2017); (c) and (d) were inspired by Nicol et al. (2016).

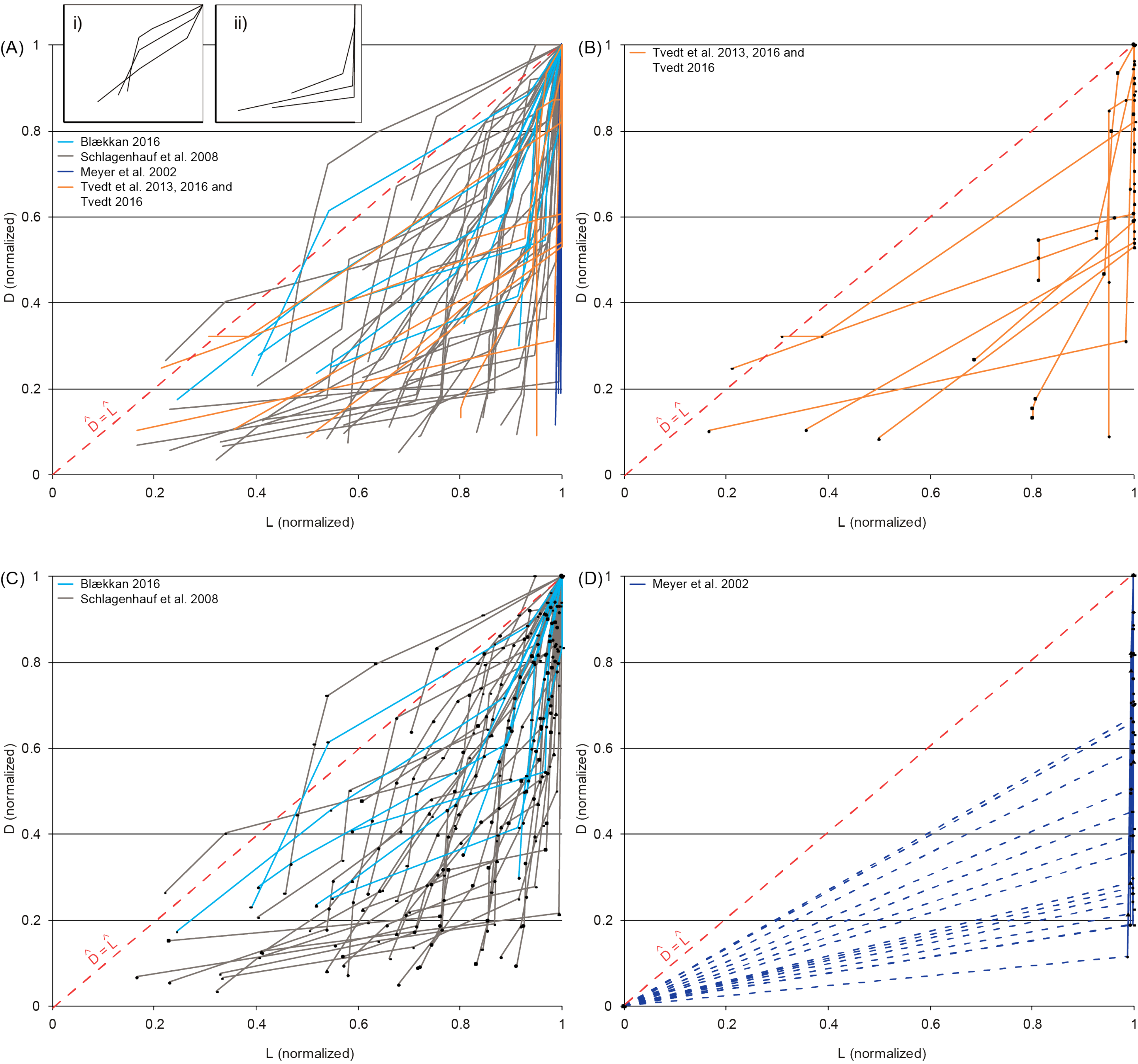

Figure 2. Normalized maximum displacement (D) versus normalized fault length (L) plots though fault life for a series of faults. (A) shows data from all faults studied herein, whereas (B), (C), and (D) show selections of the data. The data includes natural faults from Tvedt et al. (2013, 2016), Tvedt (2016), Meyer et al. (2002), faults from plaster experiments by Blækkan (2016) and faults from sandbox experiments by Schlagenhauf et al. (2008). Note that the data from Meyer et al. (2002) carries some uncertainty as the data were manually extracted from the log-log D-L plots in that paper. Inset (i) shows D-L graphs for select faults that exhibit sympathetic D-L growth, i.e. isolated fault growth. Inset (ii) shows D-L graphs from select faults that show clearly separate low-gradient and high-gradient segments, separated by clear inflection points. (B) shows data from natural faults extracted from Tvedt (2016) and Tvedt et al. (2013, 2016). (C) shows data from faults produced in physical analogue experiments from Schlagenhauf et al. (2008) and Blækkan (2016). (D) shows the data extracted from Meyer et al. (2002); note however that we have added (x, y) = (0, 0) to all the D-L curves, in order to illustrate that each of the vertical D-L graphs in Meyer et al. (2002) have an additional unrecorded and unknown growth phase that is illustrated by dashed lines. See text for full discussion.

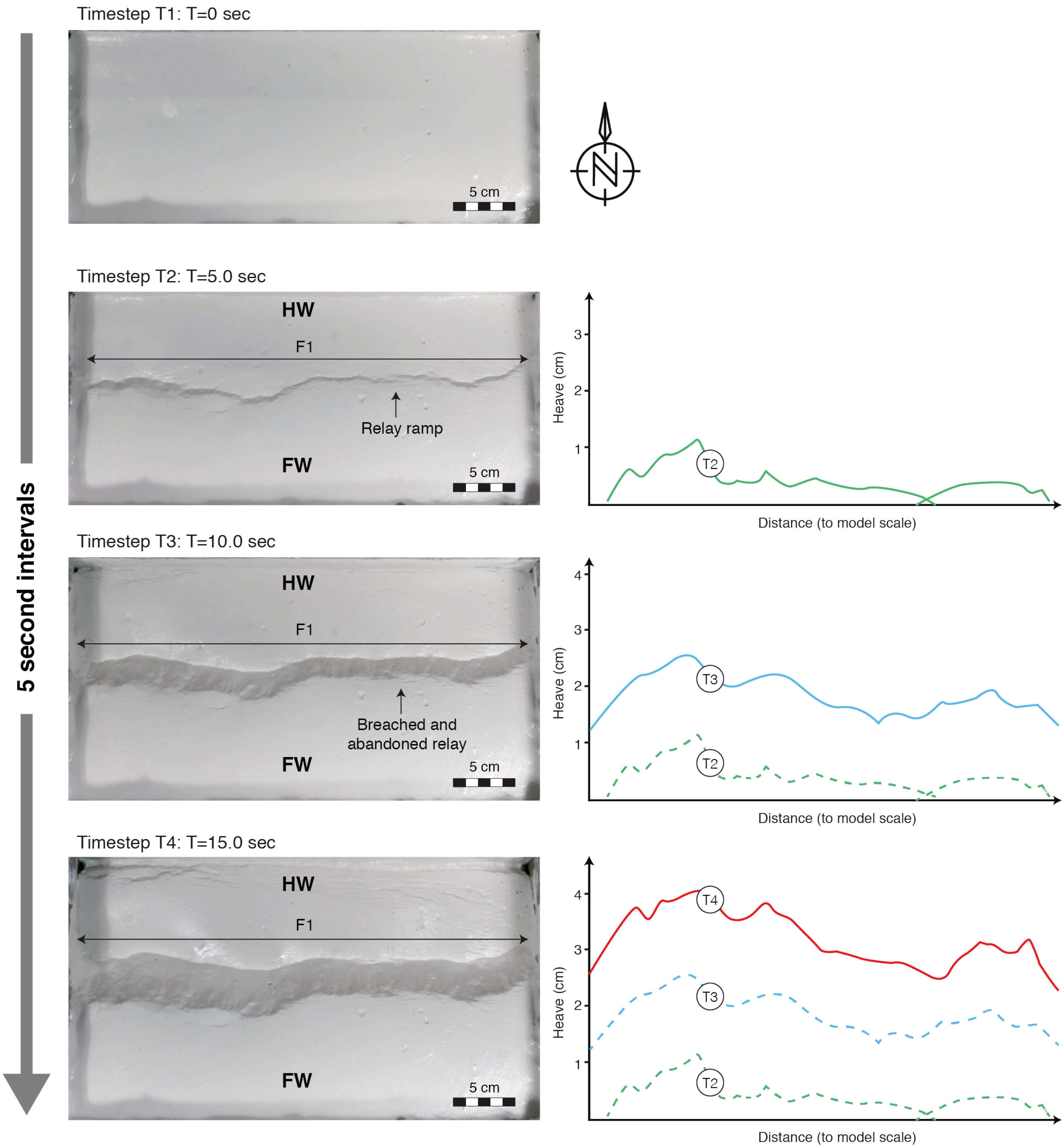

Figure 3. Plaster experiment of normal fault evolution. Four timesteps, T1 through T4 at 5 second intervals, are shown. Timestep T1 is the experiment at the onset of extension. To the right, displacement-length plots for the fault evolving in the experiment are shown for timesteps T2 (green), T3 (blue) and T4 (red). Note that the fault seen in T2 already at that stage has established itself across the extent of the model. See Figure 4 for four additional, shorter, 0.5-second timesteps immediately prior to timestep T2, which show the lengthening phase of the fault.

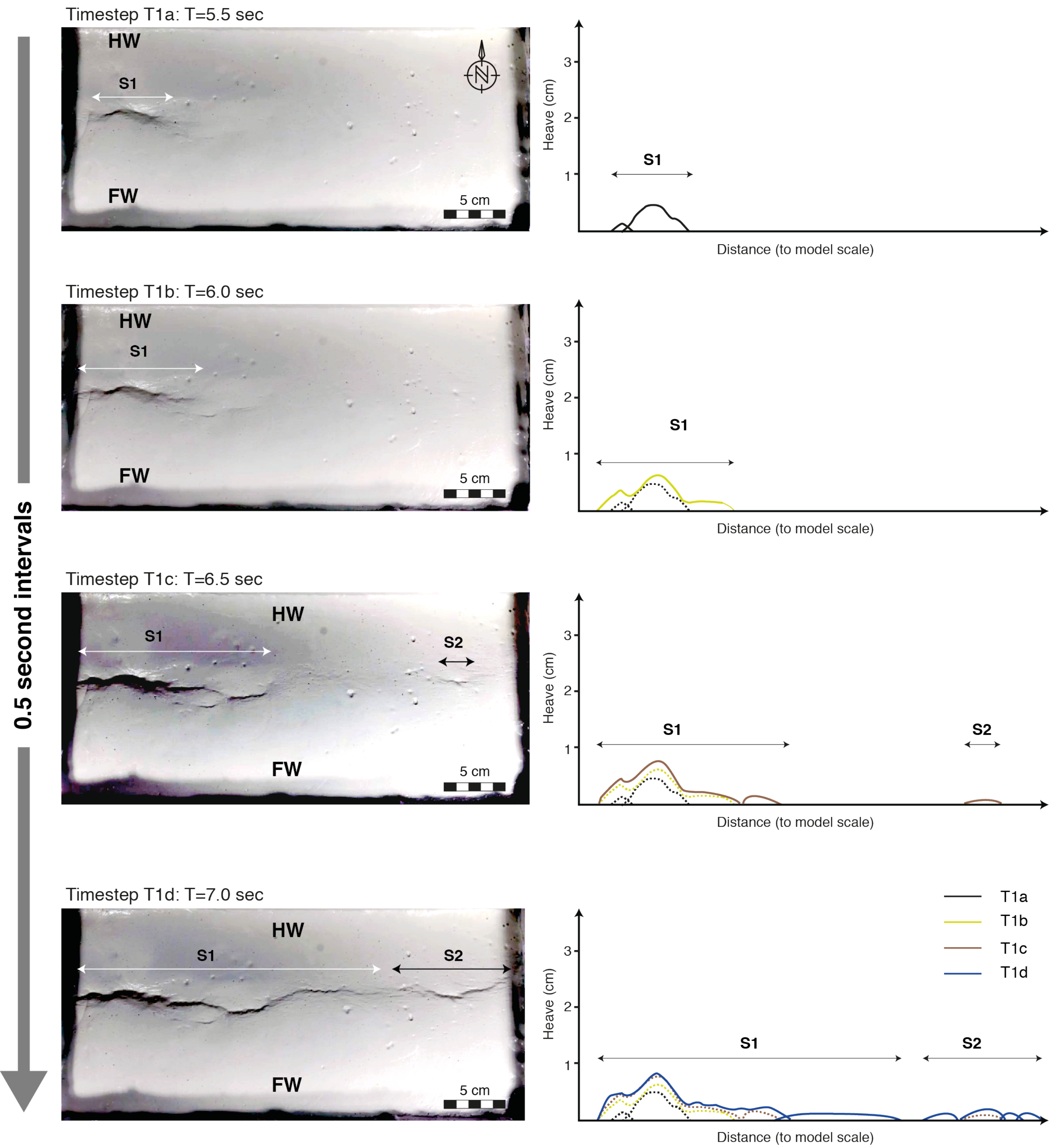

Figure 4. Plaster experiment of normal fault evolution; 4 timesteps are shown at 0.5 second intervals; T1a through T1d. These timesteps cover the 2 seconds leading up to timestep T2 in Figure 3; see Figure 3 caption for further explanation.

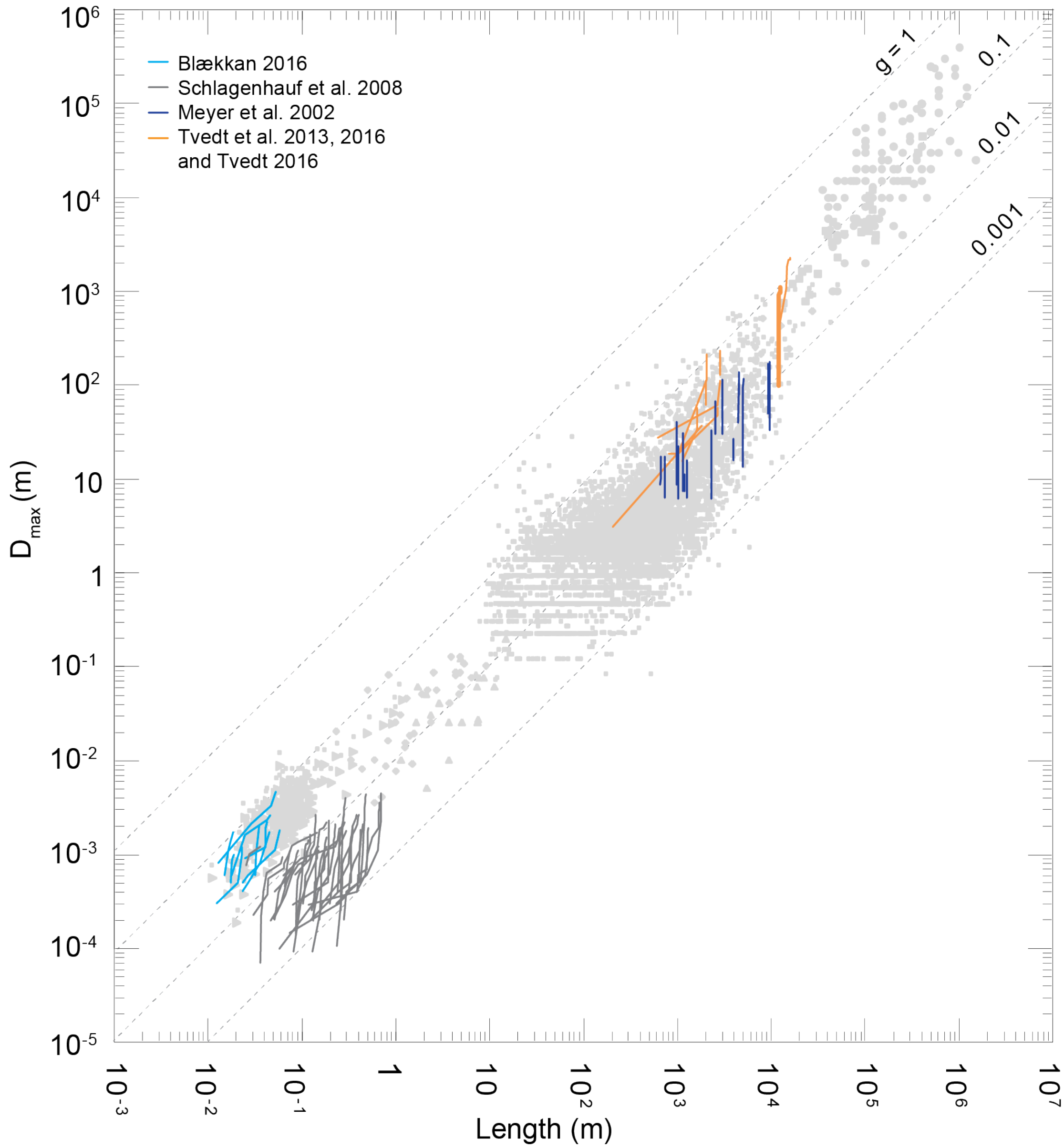

Figure 5. Global D-L dataset (grey data points) for faults plotted in log-log space (D-L data extracted from Krantz 1988; Gudmundsson and Bäckström 1991; Cowie and Scholz 1992a, and references therein; Dawers et al., 1993; Cartwright et al., 1995; Schlische et al., 1996; Schultz and Fossen 2002). The D-L paths shown in Figure 2 of this study are also shown. Note most of the different D-L paths from this study plot within the global dataset, despite that these growth paths show a wide range of behaviours (see text for full discussion). This demonstrates that the global correlation of D and L cannot be invoked to support 'isolated' fault growth, since 'constant-length' and hybrid growth patterns are all fully consistent with, and may hide within, the global D-L database as shown here.

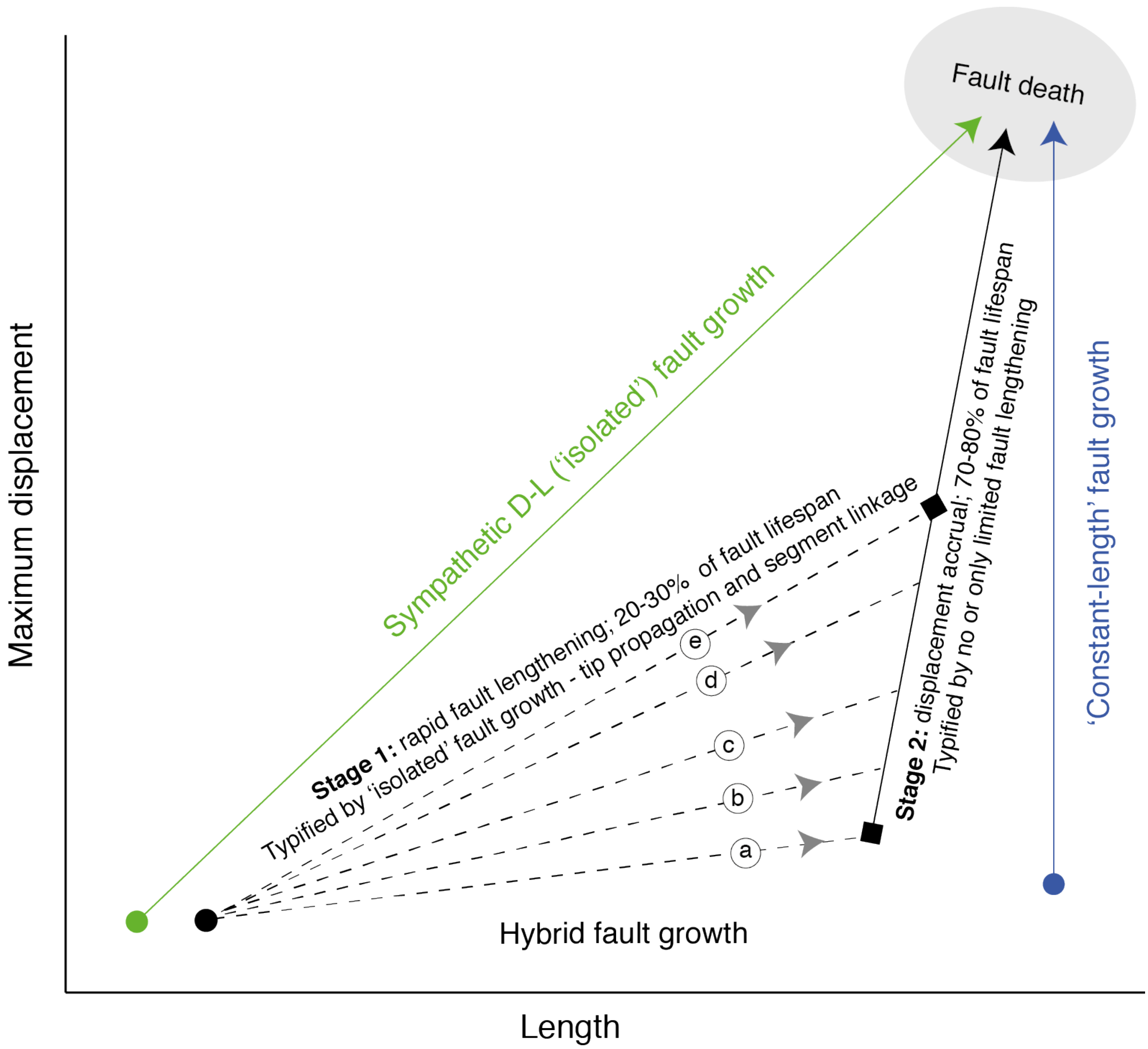

Figure 6. Schematic illustration showing idealized D-L growth trajectories of the end member 'isolated' (green) and 'constant-length' (blue) fault models, as well as a series of hybrid-type fault growth trajectories (black). As shown in this paper, few faults follow the isolated or constant-length trajectories; most faults follow D-L growth paths that are characteristic of a hybrid growth mode characterized by two stages. The first stage is characterized by rapid fault lengthening and a variable amount of displacement accrual, and is best described by the isolated model since it is associated with lengthening achieved by tip propagation, relay formation and breakdown, segment linkage and amalgamation to ultimately establish near-full fault lengths at the end of Stage 1. The second stage (Stage 2), is best described as 'constant-length' fault behaviour, i.e. displacement accrual without significant tip propagation or further fault lengthening. The fault growth trajectory in D-L space during Stage 1 of the hybrid growth model varies significantly, from sub-horizontal coherent-like trajectories with limited displacement accrual (graph a), to steep and isolated-like trajectories with significant displacement accrual during Stage 1 (graph e). See text for full discussion.